Inorganic Chemistry

ARTICLE

pubs.acs.org/IC

A Model of Spin Crossover in Manganese(III) Compounds: Effects of Intra- and Intercenter Interactions

Sophia I. Klokishner,* Marianna A. Roman, and Oleg S. Reu

Institute of Applied Physics, Academy of Sciences of Moldova, Kishinev, Moldova

ABSTRACT: A microscopic approach to the problem of cooperative spin crossover in the $[MnL2]NO_3$ crystal, which contains Mn^{III} ions as structural units, is elaborated on, and the main mechanisms governing this effect are revealed. The proposed model also takes into account the splitting of the low-spin $^3T_1$ (t_2^4) and high-spin ^5E (t_2^3e) terms by the low-symmetry crystal field. The low-spin → high-spin transition has been considered as a cooperative phenomenon driven by interaction of the electronic shells of the Mn^{III} ions with the all-around full-symmetric deformation that is extended over the crystal lattice via the acoustic phonon field. The model well explains the observed thermal dependencies of the magnetic susceptibility and the effective magnetic moment.

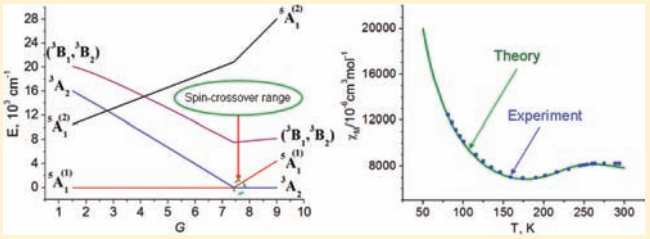

1. INTRODUCTION

The spin-crossover phenomenon was first discovered by Cambi et al. on a series of iron(III) tris(dithiocarbamate) compounds more than 70 years ago.[1−3] The phenomenon is referred to as transitions from high-spin (hs) to low-spin (ls) or from ls to hs states in octahedral transition-metal complexes with d^4, d^5, d^6, and d^7 electronic configurations. These states possess different orbital and spin multiplicities. Spin crossover is one of the best examples of molecular bistability, which means that in some transition-metal complexes the spin state of the complexes changes due to external perturbation such as temperature, pressure, and light irradiation. The bistable compounds could be useful for the construction of memory and sensory molecular-based devices. In the literature, numerous compounds of Fe^{II}-($3d^6$), Fe^{III}($3d^5$), and Co^{II}($3d^7$) exhibiting spin crossover both in the solid state and in solution have been reported.[4−9] The main characteristic of spin crossover is the temperature dependence of the population of the hs state (hs fraction). Depending on the shape of this curve, the transitions are divided into the following groups: gradual transitions that occur over an extended temperature range, abrupt transitions that take place within a narrow temperature range, transitions associated with a thermal hysteresis loop or with a two-step process, and incomplete transitions.[5] The two most important observed consequences of a spin transition are changes in the metal−ligand bond lengths accompanying the repopulation of the t_2 and e orbitals and changes in the magnetic properties. For iron compounds, the spin conversion also clearly manifests in the Mössbauer spectra. For the description of spin-crossover iron(II) compounds, the semiempirical thermodynamic approach,[10] the Wainflasz and Pick model, and its extensions, called "Ising-like models", are very often applied.[11−18]

Only in a few cases is spin crossover observed for chromium(II) and manganese(III)[19−22] compounds. Some manganese(III) complexes reported in ref 23 were not structurally characterized, and probably, therefore, the observed temperature dependence of their magnetic moment was attributed to exchange interactions. However, in ref 24, an assumption was made that the more likely interpretation of this dependence is spin crossover. [Mn(trp)] (trp^{3-} = tris[1-(2-azolyl)-2-azabuten-4-yl]amine) represents a well-characterized example of spin conversion in Mn^{III} ions,[19] which continues to attract the attention of researchers.[25−27] Heat capacity and magnetic susceptibility measurements show that the spin transition from the hs state to the ls state in $[Mn^{III}(pyrol)_3tren]$ {($Hpyrol)_3$tren = tris[1-(2-azolyl)-2-azabuten-4-yl]}[19,25] occurs abruptly at about 44 K. Paraelectric behavior due to a dynamic Jahn−Teller effect has been found in the hs phase above T_c = 48 K of the manganese(III) spin-crossover complex [Mn(taa)] (H_3taa = tris[1-(2-azolyl)-2-azabuten-4-yl]amine).[28] The dielectric constant of this compound obeys the Curie−Weiss law with an asymptotic Curie temperature at 26 K, suggesting competition between a ls phase and a ferroelectrically ordered phase at low temperatures. Recently, it was observed that modulation of the orientation of the $N_4(O^-)_2$ donors in a series of hexadentate ligands has a dramatic effect on the spin state of manganese(III) complexes and that gradual thermal spin crossover may be attained when the phenolate oxygen donors are trans to each other.[24] In fact, by variation of the length of the alkyl chains in the starting tetraamine, such a geometry was achieved. A manganese(III) complex possessing a hs ground state at all temperatures was obtained with the aid of a triethylene−tetraamine link (L_1), which orients the oxygen donors cis to each other. At the same time, lengthening of the tetraamine link by two methylene groups (L2) led to a trans geometry of the oxygen donors, facilitating spin crossover[24] in the $[MnL2]NO_3$ compound. An axially compressed octahedral geometry for the Mn^{III} ion in the mixed nitrogen−oxygen ligand surrounding (MnN_4O_2) has been reported in 29. The magnetic

Received: May 15, 2011
Published: October 25, 2011

susceptibility of the complex clearly exhibits spin crossover. Recently, magnetic measurements and variable-temperature single-crystal X-ray crystallography proved spin-crossover effects in the [Mn(5-Br-sal-N-1,5,8,12)]ClO_4 compound.[30]

The vibrational contribution to the entropy change ΔS of the ls ($^3T_1$) to hs (^5E) spin transition in the $3d^4$ octahedral system [Mn^{III}(pyrol)$_3$tren] has been estimated by means of density functional theory (DFT) calculations of the vibrational normal-mode frequencies in ref 31. The obtained value at the transition temperature for the Mn^{III} complex is $\Delta S_{vib}(44\ K) = 6.3\ J\ K^{-1}\ mol^{-1}$, which is approximately half of the experimentally determined 13.8 J K^{-1} mol^{-1}. In ref 28, the geometry optimization of the hs [Mn(taa)] molecule was carried out by a hybrid DFT quantum-chemical calculation. On the basis of a four-state Ising−Potts model,[32] a phase diagram incorporating both a virtual cooperative Jahn−Teller transition from the hs state to the ferroelectrically ordered phase and a spin-crossover transition hs ↔ ls was also proposed to elucidate the interrelation between these three phases of the [Mn(taa)] compound.[28] Three adjustable parameters were introduced to the model to reproduce the spin-crossover transition temperature, the virtual Jahn−Teller transition temperature, and the effective ls−hs gap. In ref 30, with the aid of DFT for the [Mn(5-Br-sal-N-1,5,8,12)]ClO_4 complex, the geometry optimization and vibration analysis have been performed and the spin and density difference maps have been obtained. From DFT calculations, parameters relevant for interpretation of the observed effect in the framework of the ligand-field paradigm have been retrieved.[30] It was obtained that the hs ground state is higher with $\Delta E \sim 2000\ cm^{-1}$ than the ls one. At the same time, in refs 28 and 30−32, the cooperative interactions, which together with the intraion ones determine the type of spin crossover and transition temperature, are not included in the model. An attempt to reveal the role of these interactions is undertaken in 28. Meanwhile, in ref 28, the interion interactions are introduced phenomenologically within the framework of the four-state Ising−Potts model.

In the present paper, we develop a microscopic theoretical approach for the description of the spin-crossover phenomenon in manganese(III) compounds, and with the aid of this approach, we explain the experimental data on the temperature dependence of the magnetic susceptibility and magnetic moment in the [MnL2]NO_3 compound.[24]

2. THE MODEL

The Mn^{III} ion possesses four electrons in the incomplete d shell. Depending on the ratio Dq/B in the cubic crystal field (where Dq is the parameter of the cubic crystal field and B is the Racah parameter), the ground state of this ion is the triplet $^3T_1$ or the doublet ^5E further on referred to as the ls and hs states, respectively. The interaction of the ground state ^5E of the Mn^{III} ion with the tetragonal Jahn−Teller vibrations of the highly symmetrical ligand surroundings leads to the situation when the system is held up in one of the minima of the lower adiabatic potential sheet, which results in distortion of the octahedral manganese complex and a lowering of its symmetry.[33] The majority of hs manganese(III) complexes subject to the Jahn−Teller effect demonstrate elongated octahedral surroundings. In this case, one inevitably faces the problem of finding out the initial equilibrium configuration of the complex. Unfortunately, this problem cannot be solved in an unique way. Therefore, usually a simplified model is applied that assumes that the observed distortion of the manganese(III) complexes is a result of the action of a low-symmetry crystal field.

Table 1. Spherical Coordinates of the Ligands in the MnN_4O_2 Complex in the [MnL2]NO_3 Compound

	ligand					
	1	2	3	4	5	6
R_i, Å	1.988	1.988	2.050	2.050	1.872	1.872
θ_i, rad	$\pi/2$	$\pi/2$	$\pi/2$	$\pi/2$	0	π
φ_i, rad	0	$\pi/2$	π	$3\pi/2$	0	0

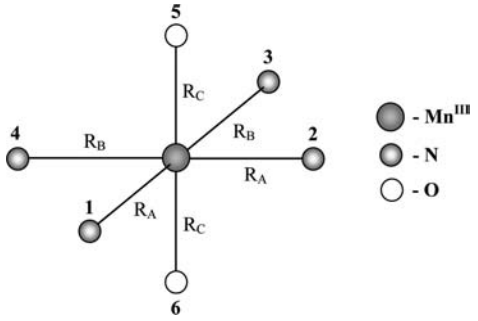

Figure 1. Ligand surroundings of the Mn^{III} ion in the [MnL2]NO_3 compound.

Inspection of the molecular structure and interatomic distances (Table 1) reveals that in the [MnL2]NO_3[24] complex the Mn^{III} ion has a quasi-octahedral environment made up by four nitrogen and two oxygen atoms (Figure 1). With an increase in the temperature, the Mn−N bond lengths increase, while the axial Mn−O bond lengths remain almost the same. In the temperature range 100−300 K, the symmetry of the [MnL2]NO_3 complex[24] does not change and the complex may be approximately regarded as a system belonging to the C_{2v} point group. The structure of the [MnL2]NO_3 complex differs from that for manganese(III) complexes subject to strong Jahn−Teller effect because this complex is compressed along the O−Mn−O direction. This difference, along with the conserved symmetry of the complex in a wide temperature range, allows one to suppose that the cooperative interaction facilitating the spin transition is apparently not of the Jahn−Teller nature. At the same time, in order to avoid the solution of the Jahn−Teller problem for an isolated complex, we assume that distortion of the nearest surrounding of the Mn ion comes from a low-symmetry crystal field.

The Hamiltonian of the system of interacting Mn ions

$$H = \sum_n V_{cr}^n + \sum_n V_{ee}^n + V_{st} \qquad (1)$$

includes the crystal fields (V_{cr}^n) acting on the Mn ions, the interelectronic repulsion (V_{ee}^n) inside each Mn ion, and the electron−deformational cooperative interaction between the Mn ions, which facilitates the spin transition.

2.1. Crystal Field. We employ the exchange-charge model of the crystal field[34−39] that takes into account two contributions to the energy of the Mn^{III} ion in the crystal field, namely, the contribution arising from interaction of the electrons in the d shell with the point charges (pc) of the surrounding ligands and the contribution coming from the overlap of the 3d orbital with the

dx.doi.org/10.1021/ic201025u |Inorg. Chem. 2011, 50, 11394–11402

Table 2. Numerical Values of the Overlap Integrals $S_l(R)$, Their Derivatives $S'_l(R)$, and Crystal-Field Parameters B_l^m as a Function of the Parameter G

$S_2(R_A)$	$S_4(R_A)$	$S_2(R_B)$	$S_4(R_B)$	$S_2(R_C)$	$S_4(R_C)$
0.0169	0.0107	0.0140	0.0091	0.0201	0.0128
$S'_2(R_A)$ (in a_0^{-1})[a]	$S'_4(R_A)$ (in a_0^{-1})	$S'_2(R_B)$ (in a_0^{-1})	$S'_4(R_B)$ (in a_0^{-1})	$S'_2(R_C)$ (in a_0^{-1})	$S'_4(R_C)$ (in a_0^{-1})
−0.0275	−0.0138	−0.0233	−0.0127	−0.0350	−0.0180
B_2^0, cm^{-1}			B_4^0, cm^{-1}		B_4^4, cm^{-1}
40374 + 3426G			6444 + 9818G		4307G

[a] a_0 is the Bohr radius.

ligand orbitals. The latter is referred to as the contribution of exchange charges (ec; see the Appendix). In this model, the crystal-field operator written in the frame of reference shown in Figure 1 is as follows:

$$V_{cr} = B_2^0 Y_{2,0} + B_4^0 Y_{4,0} + B_4^4 (Y_{4,-4} + Y_{4,4}) \quad (2)$$

where the parameters B_l^m are determined as

$$B_2^0 = -\frac{4e^2\sqrt{\frac{\pi}{5}}}{R_A R_B {R_C}^3}[-R_A R_B\langle r^2\rangle + G{R_C}^2[R_B R_C S_2(R_A) + R_A R_C S_2(R_B) - 2R_A R_B S_2(R_C)]]$$

$$B_4^0 = -\frac{e^2\sqrt{\pi}}{15 R_A R_B {R_C}^5}[40 R_A R_B\langle r^4\rangle + 9G{R_C}^4[3R_B R_C S_4(R_A) + 3R_A R_C S_4(R_B) + 8R_A R_B S_4(R_C)]]$$

$$B_4^4 = -\frac{3e^2 G\sqrt{\frac{7\pi}{10}}}{R_A R_B}[R_B S_4(R_A) + R_A S_4(R_B)] \quad (3)$$

The expressions (3) have been obtained by taking into account that in the compound under examination the point charges of oxygen and nitrogen ligands are equal to e and 0, respectively. Actually, to get accurate values of atomic charges, a calculation of the full electronic structure of the crystal is needed, which represents a separate problem. Here the numerical values of the ligand point charges have been identified approximately with the oxidation states and determined from the following considerations. Because the oxidation state of the counterion NO_3 is 1−, the complex MnL2 has in total a positive oxidation state 1+ and consists of a Mn^{III} ion and a L2 ligand having the oxidation state 2−. The only acidic hydrogen atoms in the L2 ligand are those attached to the oxygen atoms. Therefore, the protons H^+ on OH are lost, giving two negative oxidation numbers on the two oxygen atoms, and the oxidation states of the nitrogen atoms are vanishing. The spherical coordinates of the ligands are given in Table 1. In subsequent calculations for the Mn^{III} ion, the values $\langle r^2\rangle$ = 1.286 a.u., $\langle r^4\rangle$ = 3.446 a.u. have been used.[40] Numerical values of the overlap integrals $S_l(R_C)$,$S_l(R_B)$, and $S_l(R_C)$ (Table 2) have been computed with the aid of the radial 3d wave functions of Mn^{III} and the 2s,2p functions of oxygen and nitrogen given in ref 41. The parameters B_2^0, B_4^0, and B_4^4 (Table 2) as functions of the parameter G have been estimated with the aid of formulas (3) and the overlap integrals. Actually, such a representation allows one to determine the partial contributions that come to the parameters B_l^m from the exchange and point charges of the crystal field. Further on the value of the parameter G will be obtained from the optimal coincidence between the calculated and observed temperature dependences of the magnetic susceptibility and effective magnetic moment.

Now let us focus on the problem of the basis set. The crystal field of C_{2v} symmetry (eq 2) acting on the Mn ions may produce significant splitting of the cubic terms of the Mn^{III} ions, thus changing the mutual arrangement of the levels. In this field, the hs $^5E(t_2^3e)$ term splits into two nondegenerate states that are not mixed with any other states by Coulomb interaction because the configuration d^4 gives only one cubic E level with spin S = 2. On the other hand, the configurations t_2^4, t_2^3e, $t_2^2e^2$, and t_2e^3 give rise to seven $^3T_1$ levels.[42] To properly reproduce the energies of the low-lying Stark levels arising from splitting of the ls $^3T_1(t_2^4)$ term, we include in the basis set the following states:

$$^3T_1(t_2^4),\ ^3T_1(t_2^3(^2T_2)e),\ ^3T_1(t_2^3(^2T_1)e),\ ^3T_1(t_2^2(^3T_1)e^2(^1A_1)),\ ^3T_1(t_2^2(^3T_1)e^2(^1E)),\ ^3T_1(t_2^2(^3T_1)e^2(^3A_2)),\ ^3T_1(t_2e^3) \quad (4)$$

and take into account interaction of these states with the crystal field (2) as well as their Coulomb mixing.[42] The wave functions of states (4) are quoted in the Appendix. Because the Racah parameters in a crystal are reduced compared to those for free ions due to the covalency of the Mn^{III}−ligand bonds (the so-called nephelauxetic effect; see, for instance, ref 43) in calculations, we take for the parameters B and C values that make up 80% of the free-ion values. The calculations apparently show that in a wide range of parameter G values the effect of mixing of the $^3T_1(t_2^4)$ state with the other six $^3T_1$ states (4) is comparatively small for the Mn^{III} ion in the mixed-ligand surrounding, and the low-lying energy spectrum of this ion consists of four levels predominantly arising from the splitting of the $^3T_1(t_2^4)$ and $^5E(t_2^3e)$ states by the crystal field (Figure 2). These levels transform according to the irreducible representations A_2,(B_1, B_2), $A_1^{(1)}$,$A_1^{(2)}$ of the C_{2v} point group (Figure 2); the energies of the states $^3B_1$ and $^3B_2$ coincide. From Figure 2, it is seen that for parameter G values of less than 2.78 the ground state is the $^5A_1^{(1)}$ level while the first excited state is the $^5A_1^{(2)}$ level. With an increase of G, the energy of the state $^3A_2$ becomes lower than that of the $^5A_1^{(2)}$ state, but the ground state remains the same. At the point G = 7.42, the change of the ground state takes place. In the range of parameters G > 7.42, the ground state $^3A_2$ and excited state $^5A_1^{(1)}$ belong to spin values S = 1 and 2, respectively. The range of parameters G > 7.42 is favorable for spin crossover in the $[MnL2]NO_3$ compound. In fact, the observed magnetic moment[24] increases from 2.8 μ_B at 80 K to 4.4 μ_B at 300 K, indicating thus the change of the ground-state spin from 1 to 2. It

dx.doi.org/10.1021/ic201025u |Inorg. Chem. 2011, 50, 11394–11402

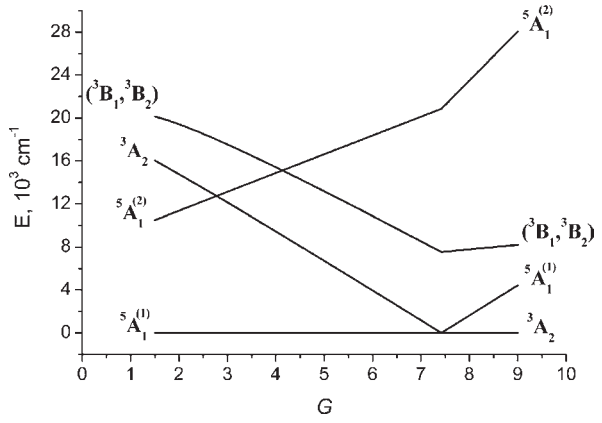

Figure 2. Energies of the low-lying levels of the Mn^{III} ion in the MnN_4O_2 complex as a function of the exchange-charge model parameter *G*.

should be also noted that in the range of parameters *G*, wherein spin crossover may take place (Figure 2), the energy gaps between the excited $(^3B_1,^3B_2)$,$^5A_1^{(2)}$ and low-lying $^3A_2$ and $^5A_1^{(1)}$ levels exceed significantly *kT*. Thus, the low-lying spectrum consists of two levels, ls $^3A_2$ and hs $^5A_1^{(1)}$, well separated from other excited-state levels arising from the splitting of the cubic $^3T_1$ and ^5E terms.

Finally, we discuss the role of spin−orbital (SO) interaction. This interaction[42] mixes the cubic $^3T_1$ and ^5E terms and splits the $^3T_1$ term. Generally speaking, the SO interaction should be included in the electronic single-ion Hamiltonian along with the low-symmetry crystal-field operator. However, because of the local Jahn−Teller effect in each Mn ion, freezing of the orbital momentum, i.e., reduction of the SO interaction, takes place.[44−46] Because for a Mn ion the free-ion SO constant $\lambda = 80$ cm^{-1} [40] is sufficiently small, one can assume that the SO interaction reduced by the Jahn−Teller effect[44−46] as well as by strong covalence effects (see ref 42 and Table 2) will lead to splittings of the cubic Mn^{III} terms, negligible compared to the effective gap Δ_{hs} between the hs and ls states in the low-symmetry C_{2v} crystal field (see Figure 2 and section 3). Therefore, the effects of the SO interaction are not examined.

2.2. Electron−Deformational Interaction. The spin transformation in the compound under examination does not cause a change in the crystal symmetry. Therefore, the spontaneous strain accompanying the spin conversion is assumed to be full symmetric and to appear as a consequence of occupation of the antibonding e orbital in the Mn^{III} ion. Taking into account that in spin-crossover compounds the medium between the molecules is more easily affected by deformation than that inside the molecule in the subsequent examination, a difference is made between the molecular and intermolecular space. As in refs 47−49, we introduce the internal molecular $\varepsilon = (\varepsilon_{xx}^1 + \varepsilon_{yy}^1 + \varepsilon_{zz}^1)/3^{1/2}$ and external (intermolecular volume) $\varepsilon_2 = (\varepsilon_{xx}^2 + \varepsilon_{yy}^2 + \varepsilon_{zz}^2)/3^{1/2}$ strains and, corresponding to these full-symmetric strains, bulk moduli c_1 and c_2. In each molecule, we consider interaction of the Mn^{III} ion with the arising ε_1 strain. Within the framework of Kanamori's approach,[50] the contribution of uniform strains ε_1 and ε_2 in the crystal Hamiltonian can be set by the operator

$$H_{st} = \frac{Nc_1\Omega_0{\varepsilon_1}^2}{2} + \frac{Nc_2(\Omega - \Omega_0){\varepsilon_2}^2}{2} + \nu_1\varepsilon_1\sum_n \tau_n + \nu_2\varepsilon_1 N \quad (5)$$

where Ω_0 and Ω are the molecular and unit cell volumes, respectively, *N* is the number of unit cells in the crystal, $\nu_1 = (\nu_{hs} - \nu_{ls})/2$, $\nu_2 = (\nu_{hs} + \nu_{ls})/2$, where ν_{hs} and ν_{ls} are the constants of interaction of the Mn^{III} ion with the full-symmetric strain ε_1 in the hs $^5A_1^{(1)}$ and ls $^3A_2$ states, respectively. In eq 5, the first two terms describe the elastic energy of the deformed crystal, and the third and fourth terms correspond to coupling of the d electrons of the Mn^{III} ion with the uniform deformation ε_1. In the basis of the hs and ls states, the 8 × 8 matrix τ_n is diagonal, and its matrix elements 1 and −1 correspond to the states $^5A_1^{(1)}$ and $^3A_2$. For a uniform crystal compression (or extension), the relation of ε_2 to ε_1 is roughly supposed to be

$$\varepsilon_2 \approx \varepsilon_1\frac{c_1}{c_2} \quad (6)$$

If we replace the molecular and intermolecular volumes by coupled parallel springs, the same relation will hold. With account of eq 6 after minimizing eq 5 over the strain ε_1, we obtain

$$H_{st} = -b\sum_n \tau_n - \frac{J}{2N}\sum_{n,m}\tau_n\tau_m \quad (7)$$

where

$$b = A\nu_1\nu_2, \quad J = A{\nu_1}^2, \quad A = \frac{c_2}{c_1[c_2\Omega_0 + c_1(\Omega - \Omega_0)]} \quad (8)$$

Thus, the coupling to the strain gives rise to an infinite-range interaction between all Mn ions of the crystal. It should be mentioned that the model of the elastic continuum, introduced above, satisfactorily describes only the long-wave acoustic vibrations of the lattice. Therefore, the obtained intermolecular interaction, in fact, corresponds to the exchange via the field of long-wave acoustic phonons. If $c_1 = c_2$, the Hamiltonian of intermolecular interaction acquires the form generally accepted in the theory of the cooperative Jahn−Teller effect.[50,51] Provided that $c_1 \gg c_2$ and $\nu_1 \sim c_1$, the interaction term in eq 7 corresponds to that obtained in the model of elastic interactions.[4] The first term in eq 7 also arises from the interaction with the deformation and acts as an additional field applied to each spin-crossover molecule.

2.3. Mean-Field Approximation. For a system of interacting spin-crossover Mn ions, the solution of the problem can be obtained in the framework of the mean-field approximation. In this approximation, the Hamiltonian H_{st} decomposes into the sum of single-ion Hamiltonians

$$\tilde{H}_{st} = \sum_n H_{st}^n, \quad H_{st}^n = -(B + J\bar{\tau})\sum_n \tau_n \quad (9)$$

where $\bar{\tau} = \langle\tau\rangle$ is the thermal average of the operator τ. Then, taking into account eq 9, we obtain the total Hamiltonian for a single Mn^{III} ion

$$H_n = H_{st}^n + \frac{\Delta}{2}\tau_n \quad (10)$$

where Δ is the crystal-field gap between the hs $^5A_1^{(1)}$ and ls $^3A_2$ states (Figure 2). Using the eigenvalues $\varepsilon_{hs} = \Delta/2 - B - J\bar{\tau}$ and $\varepsilon_{ls} = -\Delta/2 + B + J\bar{\tau}$ of the Hamiltonian H_n, the following expression can be written for the free energy of a single

dx.doi.org/10.1021/ic201025u |*Inorg. Chem.* 2011, 50, 11394–11402

Mn ion in the molecular field:

$$F(T) = -kT\ln\{g\exp[-[\Delta_{hs}-J(2n_{hs}-1)]/kT] + \exp[-J(2n_{hs}-1)/kT]\} - \frac{\Delta_{hs}}{2} - kT\ln g_{ls} + J(2n_{hs}-1)^2/2 \quad (11)$$

where n_{hs} is the hs fraction or the total population of the hs state connected with the mean value of the order parameter by the relation $2n_{hs} - 1 = \bar{\tau}$ and $\Delta_{hs} = \Delta - 2b$ is the effective gap between the hs and ls states in the presence of cooperative interaction. It is seen that the parameter $-2b$ only redefines the crystal-field gap Δ. Finally, $g = g_{hs}/g_{ls}$, where g_{hs} and g_{ls} are the degeneracies of the hs and ls states, respectively. The two states have different degeneracies because of the different spin multiplicities and of the different densities of vibrational states associated with them.[13,14] The entropy change ΔS is connected with the ratio g_{hs}/g_{ls} by the relation[52] $\Delta S = R\ln g_{hs}/g_{ls}$. This change upon conversion is noticeable and contains vibrational contributions.[53,54]

Minimizing the free energy $F(T)$ per one crossover Mn ion over n_{hs}, we obtain a self-consistent equation for the hs fraction:

$$\frac{g\exp[-[\Delta - {}^{hs}J(2n_{hs}-1)]/kT] - \exp[-J(2n_{hs}-1)/kT]}{g\exp[-[\Delta_{hs}-J(2n_{hs}-1)]/kT] + \exp[-J(2n_{hs}-1)/kT]} = 2n_{hs}-1 \quad (12)$$

The equation obtained for the hs fraction has a set of nontrivial solutions determined by different relations between the characteristic internal parameters of the system.

2.4. Parameter Values. Magnetic Susceptibility of a Manganese Complex in the Mean-Field Approximation. We start with the estimation of the characteristic parameter J of electron–deformational interaction (eqs 7 and 8). Because the nuclear configuration is consistent with the electronic state of a manganese(III) complex, each electronic state possesses its equilibrium lattice configuration. Upon passing from one electronic state to another one, vibrational relaxation occurs in the final electronic state, and the nuclei start oscillating near the new equilibrium positions. The transition of the manganese(III) complex from the ground-state ls $^3A_2$ to the excited-state hs $^5A_1^{(1)}$ is accompanied by a change in ΔR in the Mn–N bond lengths. If the nearest surrounding of the Mn-ion (MnN_4O_2) is assumed to be pseudooctahedral, this change is approximately connected with the equilibrium positions of the nuclei in the hs Mn state by the relation[49]

$$v_{hs} - v_{ls} = \sqrt{6f\hbar\omega}\Delta R \quad (13)$$

Here v_{hs} and v_{ls} are the constants characterizing the coupling of the Mn^{III} ion in the hs and ls states with the full-symmetric vibration of the ligand surrounding, respectively, and f is the mean force constant for this vibration. The constant ν_1 of the interaction of the Mn^{III} ion with the full-symmetric strain ε_1 (eq 5) is connected with the parameter $v_{hs} - v_{ls}$ by the following relation:[49]

$$\nu_1 = \frac{v_{hs} - v_{ls}}{2}\sqrt{\frac{2f}{\hbar\omega}}R_0 = \sqrt{3}fR_0\Delta R \quad (14)$$

where R_0 is the mean value of the ligand radii for the MnN_4O_2 complex. Estimating the parameter J, we also take into account that in spin-crossover compounds the main change in the volume falls on the intermolecular space, i.e., $c_1 \gg c_2$ and the value ΔR for the manganese(III) complex varies in the range 0.08–0.11 Å.[24] Thus, for typical values $c_2 = 10^{11}$ dyn cm^{-2}, $c_2 \approx 0.1c_1$, $R_0 = 1.97$ Å, $f = 3\times10^5$ dyn cm^{-1}, $\Omega \approx 650$ Å^3,[24] $\mathbf{\Omega} = 8$ Å^3, and $\Delta R = 0.08$–0.11 Å, the parameter $J = A\nu_1^2$ falls into the range 70–95 cm^{-1}. The obtained value of J appears to be reasonable because for rare-earth zircons exhibiting the Jahn–Teller effect the constant of electron–deformational interaction is of the order of 10 cm^{-1}.[51] Then we estimate the change Ω_{hl} of the unit-cell volume under the ls → hs transition

$$\Omega_{hl} = -\frac{2\sqrt{3}}{c_1}\nu_1 = 40\ \text{Å}^3 \quad (15)$$

This value also falls within the experimental limits.[24] In such a way, the model gives reasonable values for the microscopic parameter J and the change of the unit-cell volume. The parameters g and Δ_{hs} will be obtained below from the optimal coincidence of the calculated and observed values of the magnetic susceptibility and effective magnetic moment in a wide temperature range. It is clear that the fitting procedure is restricted to the range of parameters $\Delta_{hs} > 0$ and $g > 0$.

The energy levels in the mean-field approximation and the temperature dependence of the hs fraction are used for calculation of the magnetic moment of the manganese complex with the aid of the van Vleck formula:

$$\mu^2 = g_S{}^2\mu_B{}^2\frac{6g\exp(-\varepsilon_{hs}/kT) + 2\exp(-\varepsilon_{ls}/kT)}{g\exp(-\varepsilon_{hs}/kT) + \exp(-\varepsilon_{ls}/kT)} \quad (16)$$

The temperature dependence of the magnetic susceptibility can be easily obtained from the relation

$$\mu = \sqrt{8\chi T} \quad (17)$$

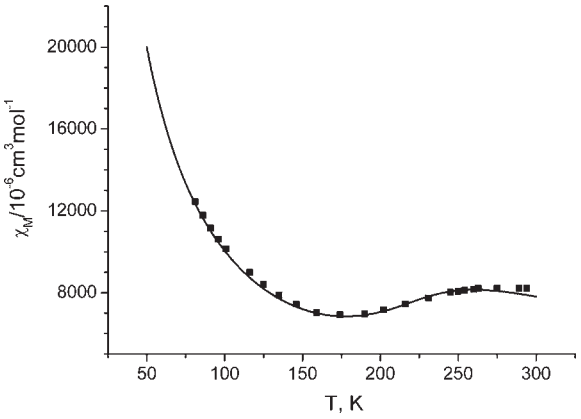

Figure 3. Temperature dependence of the magnetic susceptibility for the [MnL2]NO_3 compound: squares, experimental data;[24] solid line, theoretical fit with $g = 10$, $\Delta_{hs} = 395$ cm^{-1}, and $J = 95$ cm^{-1}.

3. RESULTS AND DISCUSSION

Figure 3 displays the observed temperature dependence of the magnetic susceptibility over the temperature range 50–300 K. The experimental room temperature value of χ is 8.22×10^{-3} cm^3 mol^{-1} [24] and decreases to 6.92×10^{-3} cm^3 mol^{-1} as the temperature is lowered to 175 K, after which temperature χ monotonically increases. The magnetic susceptibility is calculated with the set of the best fit parameters. A quite good agreement between the observed and calculated curves of the magnetic

dx.doi.org/10.1021/ic201025u |Inorg. Chem. 2011, 50, 11394–11402

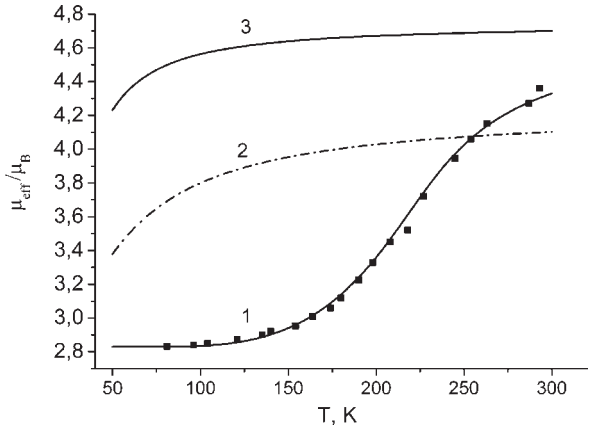

Figure 4. Variation of the effective magnetic moment of the [MnL2]-NO_3 compound as a function of the temperature: squares, experimental data;[24] (1) Theoretical fit with $g = 10$, $\Delta_{hs} = 395$ cm^{-1}, and $J = 95$ cm^{-1}. (2) Magnetic moment calculated with neglect of the electron−deformational interaction ($J = 0$) with the ratio of spin multiplicities $g = {}^5/_3$ and the crystal-field gap $\Delta = 63$ cm^{-1}. (3) Magnetic moment calculated with $J = 0$, $\Delta = 63$ cm^{-1}, and $g = 10$.

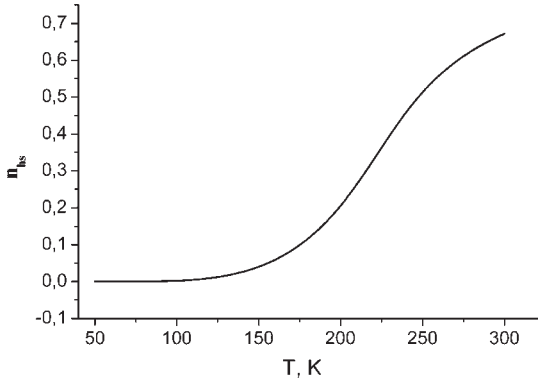

Figure 5. Population of the hs state calculated with a set of best-fit parameters $g = 10$, $\Delta_{hs} = 395$ cm^{-1}, and $J = 95$ cm^{-1}.

susceptibility is obtained. The best fit is achieved for the parameter values $\Delta_{hs} = 395$ cm^{-1}, $J = 95$ cm^{-1}, and $g = 10$ with the agreement criterion $(1/N)(\Sigma_i(\chi^i_{exp} - \chi^i_{calc})^2/(\chi^i_{exp})^2)^{1/2} = 0.017$. With the same set of parameters Δ_{hs} and g, variation of the effective magnetic moment as a function of the temperature has been calculated (Figure 4). It is seen that the model under examination also reproduces the observed magnetic moment curve. The low-temperature value of the magnetic moment corresponds to the spin $S = 1$. However, the observed magnetic moment value 4.36 μ_B at 293 K is lower than 4.9 μ_B, thus testifying a gradual incomplete spin transition in accordance with the classification accepted in ref 5. In this case, the gap between the hs and ls states significantly decreases with the temperature; however, the hs state remains higher in energy. This observation is also confirmed by Figure 5, wherein there is shown the hs fraction as a function of the temperature calculated in the mean-field approximation with the set of the best fit parameters. From Figure 5, it is seen that in the range of temperatures $T < 125$ K only the ls $^3A_2$ level is populated and $n_{hs} = 0$, and then n_{hs} gradually increases with the temperature rise. However, at room temperature, $n_{hs} < 1$.

Because experimental data on the entropy change ΔS accompanying the spin transition in the $[MnL2]NO_3$ compound are not available, we estimated the ratio $g = g_{hs}/g_{ls}$ from the observed value $\Delta S = 13.8$ J K^{-1} mol^{-1} for manganese(III) spin-crossover compounds such as [Mn(taa)] [H3taa = tris[1-(2-azolyl)-2-azabuten-4-yl]amine] and $[Mn^{III}(pyrol)_3tren]$.[25,31] The value $g = 5.3$ calculated from ΔS [31] is approximately 1.9 times smaller than that obtained from the fitting procedure for $[MnL2]NO_3$. Meanwhile, the parameter g is an intrinsic characteristic of the compound and even depends on the concentration of the spin-crossover ions.[55] This allows one to assume that the best-fit value $g = 10$ is reasonable. The obtained g value is much smaller than those for iron(II) spin-crossover compounds[55] and shows that for manganese(III) systems not all metal−ligand stretching vibrations contribute to ΔS. This result is in accordance with the estimate of the vibrational contribution to the entropy change associated with the spin transition in d^4 systems performed in ref 31. Finally, with the aid of the relation $\Delta_{hs} = \Delta - 2b = 395$ cm^{-1} and the energy level diagram presented in Figure 2, we evaluate the crystal-field gap Δ between the ls $^3A_2$ and hs $^5A_1^{(1)}$ states. Because the spin transformation is assumed to be accompanied only by the full-symmetric deformation first for this estimation, we present the matrix elements ν_{hs} and ν_{ls}, which contribute to ν_1 and ν_2 in the form

$$\nu_{ls} = \langle \text{ls } {}^3A_2 | \left(\frac{\partial W}{\partial R_A} R_A + \frac{\partial W}{\partial R_B} R_B + \frac{\partial W}{\partial R_C} R_C \right)_{R_i = R_i^{ls}} | \text{ls } {}^3A_2 \rangle \frac{1}{\sqrt{3}}$$

$$\nu_{hs} = \langle \text{hs } {}^5A_1^{(1)} | \left(\frac{\partial W}{\partial R_A} R_A + \frac{\partial W}{\partial R_B} R_B + \frac{\partial W}{\partial R_C} R_C \right)_{R_i = R_i^{hs}} | \text{hs } {}^5A_1^{(1)} \rangle \frac{1}{\sqrt{3}} \quad (18)$$

where W is the electron−nuclear potential energy (see the Appendix) and i = A, B, C. After substitution of the numerical values of the radii, overlap integrals, and their derivatives (Tables 1 and 2) into (18), the matrix elements ν_{hs} and ν_{ls} expressed in terms of the phenomenological parameter G of the exchange-charge model are as follows:

$$\nu_{ls} = 10^3(8.6 + 22.4G), \quad \nu_{hs} = 10^3(8.6 + 11.5G) \quad (19)$$

and the parameter $b = A\nu_1\nu_2$ is determined as

$$b = -(1.4 + 2.8G)G \quad (20)$$

In eqs 19 and 20, the parameters ν_{ls}, ν_{hs}, and b are given in cm^{-1}. At the same time, in the model under examination, the crystal-field gap Δ between the hs and ls states is also a function of G, as is seen in Figure 2. Therefore, with the aid of the energy level diagram presented in Figure 2 and the expression (20), the equation $\Delta(G) - 2b(G) = 395$ cm^{-1} can be solved and one obtains that $\Delta(G) = 63$ cm^{-1} and $G = 7.44$. Thus, in the crystal field, the hs level possesses a slightly higher energy compared to that of the ls level. It is worth noting that the cooperative electron−deformational interaction plays a double role. On the one hand, this interaction redefines the crystal-field gap between the hs and ls states, facilitating its increase. On the other hand, in the molecular field approximation, the energies of the hs and ls levels become temperature-dependent and the energy gap between these levels decreases with the temperature rise. In order to demonstrate with utmost clarity the role of cooperative interaction in Figure 4, we also show the magnetic moment curves calculated with neglect of this interaction. Curve 2 corresponds to $\Delta = 63$ cm^{-1} and $g = {}^5/_3$;

dx.doi.org/10.1021/ic201025u |Inorg. Chem. 2011, 50, 11394–11402

i.e., only the spin multiplicity for the hs and ls levels was taken into account. In calculations of curve 3 for Δ, the same value was taken and $g = 10$. It is obvious that both calculated curves show a slight increase of the magnetic moment in the low-temperature range. Beginning from 100 K, the magnetic moment values are practically constant. These curves do not reproduce the observed one, which shows a gradual increase of the magnetic moment in the temperature range 125−300 K.

Finally, in the same approximation with the aid of relations (19) and numerical values of the parameters c_1, c_2, Ω, and Ω_0 given above, we evaluate the parameter $J = Av_1^2 = 0.9G^2$ of the cooperative electron−deformational interaction and obtain a value of 50 cm^{-1}. Thus, both estimations of the parameter J performed with the aid of eqs 14 and 18−20, respectively, give values of the same order of magnitude, and the best-fit value falls within the estimated limits.

4. CONCLUDING REMARKS

To explain the phenomenon of spin transition in the $[MnL2]NO_3$ compound, we have reported a theoretical model. The model takes into account the low-symmetry crystal field acting on the Mn ion and the cooperative long-range electron−deformational interaction facilitating the spin transition. The inputs for the task were the structure of the complex formed by the Mn ion and its nearest surrounding, the crystal structure, and experimental data concerning the magnetic properties. The main results of the consideration can be summed up in the following way. An energy level diagram is constructed for a single Mn^{III} ion in the mixed-ligand surrounding of C_{2v} symmetry. The energies of the levels have been calculated in the exchange-charge model of the crystal field accounting for covalence effects. The range of the crystal-field parameters for which the low-lying part of the energy spectrum of the Mn^{III} ion consists of two nondegenerate levels arising from the states $^3T_1$ and ^5E, with the spin $S = 1$ state being the ground one, is determined. It is shown that in this case the ground level mainly originates from the $^3T_1(t_2^4)$ term; i.e., the situation facilitating spin crossover takes place. Cooperative long-range interactions have been shown to arise from coupling of the electronic states of the Mn^{III} ion to the full-symmetric strain. In this case, the molecular-field theory has proven to be particularly successful. The characteristic parameter of the long-range interaction has been evaluated in two different ways: microscopically in the exchange-charge model of the crystal field and semiempirically with the aid of the relation connecting the observed changes in the Mn−N bond lengths with the equilibrium positions of the nuclei in the hs Mn^{III} state. Both estimations are shown to give values of the same order of magnitude for the parameter of cooperative interaction. It is demonstrated that this interaction tends to diminish the energy gap between the ground ls and excited hs states and facilitates a gradual increase of the magnetic moment. In this case, in the mean-field approximation, the energy levels complying with the hs and ls states draw closer together with a temperature increase but do not intersect. Quite good agreement has been obtained between the calculated and experimental values of the magnetic susceptibility and effective magnetic moment. It should be noted that the model developed is also applicable for consideration of other manganese complexes demonstrating spin crossover.

Finally, we want to point out that in calculations of the point-charge contribution to the crystal-field parameters we used the values of these charges determined from electrostatic considerations. To some extent, this is corrected by fitting of the parameter G of the exchange-charge model. In a more general sense, calculation of the charge distribution on the ligands by the DFT method is required. This problem will be addressed in the future.

APPENDIX

1. Crystal-Field Operator. In the exchange-charge model, the parameters B_l^m of the crystal-field operator

$$V_{cr} = \sum_{\alpha} W(|\vec{r} - \vec{R}_{i\alpha}|) = \sum_{l,m} B_l^m Y_l^m(\vartheta, \phi) \tag{A1}$$

are represented as

$$B_l^m = B_l^{m(pc)} + B_l^{m(ec)} \tag{A2}$$

where $W(|\vec{r} - \vec{R}_{i\alpha}|)$ is the electron-nuclear potential energy, the component

$$B_l^{m(pc)} = \left(\frac{4\pi}{2l+1}\right) \sum_{\alpha} \frac{Z_\alpha e^2 \langle r^l \rangle}{(R_\alpha)^{l+1}} Y_l^m(\vartheta_\alpha, \phi_\alpha) \tag{A3}$$

is determined in the usual manner[34−39] and depends on the positions of the ligands, their effective charges, and radial integrals $\langle r^l \rangle$ for the Mn ions,[40] and $Y_{pm}(\vartheta,\varphi)$ are normalized spherical harmonics. The component $B_l^{m(ec)}$

$$B_l^{m(ec)} = \frac{8\pi e^2}{5} G \sum_{\alpha} \frac{S_l(R_\alpha)}{R_\alpha} Y_l^m(\vartheta_\alpha, \phi_\alpha) \tag{A4}$$

is proportional to a linear combination of squares of different types of overlap integrals of the 3d functions of the Mn ions and 2s,2p wave functions of the oxygen and nitrogen ligands

$$S_p(R_\alpha) = S_s{}^2(R_\alpha) + S_\sigma{}^2(R_\alpha) + \gamma_p S_\pi{}^2(R_\alpha)$$
$$\gamma_2 = 1,\ \gamma_4 = -4/3 \tag{A5}$$

Here $S_s(R_\alpha) = \langle 3d,m=0|2s\rangle$, $S_\sigma(R_\alpha) = \langle 3d,m=0|2p,m=0\rangle$, and $S_\pi(R_\alpha) = \langle 3d,m=\pm1|2p,m=\pm1\rangle$ are the overlap integrals of the 3d wave functions of Mn ions and the 2s,2p wave functions of the oxygen or nitrogen ligands and G is the phenomenological parameter of the model.

2. Wave Functions of the $^3T_1(t_2^n e^m)$ ($n + m = 4$) Terms.

$$^3T_1(t_2^4)$$
$$|^3T_{1\alpha}\rangle = -|\zeta\bar{\xi}\bar{\xi}\eta|,\quad |^3T_{1\beta}\rangle = |\xi\eta\bar{\eta}\zeta|,\quad |^3T_{1\gamma}\rangle = |\eta\zeta\bar{\zeta}\xi| \tag{A6}$$

$$^3T_1[t_2^3(^2T_2)e]$$
$$|^3T_{1\alpha}\rangle = -\frac{\sqrt{3}}{2\sqrt{2}}|\xi\eta\bar{\eta}u| - \frac{\sqrt{3}}{2\sqrt{2}}|\xi\zeta\bar{\zeta}u| - \frac{1}{2\sqrt{2}}|\xi\eta\bar{\eta}v| - \frac{1}{2\sqrt{2}}|\xi\zeta\bar{\zeta}v|$$
$$|^3T_{1\beta}\rangle = \frac{\sqrt{3}}{2\sqrt{2}}|\eta\xi\bar{\xi}u| + \frac{\sqrt{3}}{2\sqrt{2}}|\eta\zeta\bar{\zeta}u| - \frac{1}{2\sqrt{2}}|\eta\xi\bar{\xi}v| - \frac{1}{2\sqrt{2}}|\eta\zeta\bar{\zeta}v|$$
$$|^3T_{1\gamma}\rangle = \frac{1}{\sqrt{2}}|\zeta\xi\bar{\xi}v| + \frac{1}{\sqrt{2}}|\zeta\eta\bar{\eta}v|$$

dx.doi.org/10.1021/ic201025u |Inorg. Chem. 2011, 50, 11394–11402

$^3T_1[t_2^3(^2T_1)e]$

$$|^3T_{1\alpha}\rangle = -\frac{1}{2\sqrt{2}}\left|\xi\eta\bar{\eta}u\right| + \frac{1}{2\sqrt{2}}\left|\xi\zeta\bar{\zeta}u\right| + \frac{\sqrt{3}}{2\sqrt{2}}|\xi\eta\bar{\eta}v| - \frac{\sqrt{3}}{2\sqrt{2}}|\xi\zeta\bar{\zeta}v|$$

$$|^3T_{1\beta}\rangle = \frac{1}{2\sqrt{2}}\left|\eta\xi\bar{\xi}u\right| - \frac{1}{2\sqrt{2}}|\eta\zeta\bar{\zeta}u| + \frac{\sqrt{3}}{2\sqrt{2}}|\eta\xi\bar{\xi}v| - \frac{\sqrt{3}}{2\sqrt{2}}|\eta\zeta\bar{\zeta}v|$$

$$|^3T_{1\gamma}\rangle = \frac{1}{\sqrt{2}}\left|\zeta\xi\bar{\xi}u\right| - \frac{1}{\sqrt{2}}|\zeta\eta\bar{\eta}u|$$

$^3T_1[t_2^2(^3T_1)e^2(^1A_1)]$

$$|^3T_{1\alpha}\rangle = \frac{1}{\sqrt{2}}|\bar{\eta}\bar{\zeta}u\bar{u}| + \frac{1}{\sqrt{2}}|\bar{\eta}\bar{\zeta}v\bar{v}|, \quad |^3T_{1\beta}\rangle = \frac{1}{\sqrt{2}}|\bar{\zeta}\bar{\xi}u\bar{u}| + \frac{1}{\sqrt{2}}|\bar{\zeta}\bar{\xi}v\bar{v}|,$$

$$|^3T_{1\gamma}\rangle = \frac{1}{\sqrt{2}}|\bar{\xi}\bar{\eta}u\bar{u}| + \frac{1}{\sqrt{2}}|\bar{\xi}\bar{\eta}v\bar{v}|$$

$^3T_1[t_2^2(^3T_1)e^2(^1E)]$

$$|^3T_{1\alpha}\rangle = -\frac{1}{2\sqrt{2}}|\eta\zeta u\bar{u}| + \frac{1}{2\sqrt{2}}|\eta\zeta v\bar{v}| + \frac{\sqrt{3}}{2\sqrt{2}}|\eta\zeta u\bar{v}| + \frac{\sqrt{3}}{2\sqrt{2}}|\eta\zeta v\bar{u}|$$

$$|^3T_{1\beta}\rangle = \frac{1}{2\sqrt{2}}|\zeta\xi u\bar{u}| - \frac{1}{2\sqrt{2}}|\zeta\xi v\bar{v}| - \frac{\sqrt{3}}{2\sqrt{2}}|\zeta\xi u\bar{v}| + \frac{\sqrt{3}}{2\sqrt{2}}|\zeta\xi v\bar{u}|$$

$$|^3T_{1\gamma}\rangle = -\frac{1}{\sqrt{2}}|\xi\eta u\bar{u}| + \frac{1}{\sqrt{2}}|\xi\eta v\bar{v}|$$

$^3T_1[t_2^2(^3T_1)e^2(^3A_2)]$

$$|^3T_{1\alpha}\rangle = \frac{1}{\sqrt{2}}|\eta\bar{\zeta}uv| + \frac{1}{\sqrt{2}}|\zeta\bar{\eta}uv|, \quad |^3T_{1\beta}\rangle = \frac{1}{\sqrt{2}}|\zeta\bar{\xi}uv| + \frac{1}{\sqrt{2}}|\xi\bar{\zeta}uv|,$$

$$|^3T_{1\gamma}\rangle = \frac{1}{\sqrt{2}}|\xi\bar{\eta}uv| + \frac{1}{\sqrt{2}}|\eta\bar{\xi}uv|$$

$^3T_1(t_2e^3)$

$$|^3T_{1\alpha}\rangle = -\frac{\sqrt{3}}{2}|u\bar{v}v\xi| - \frac{1}{2}|v\bar{u}u\xi|, \quad |^3T_{1\beta}\rangle = \frac{\sqrt{3}}{2}|u\bar{v}v\eta| - \frac{1}{2}|v\bar{u}u\eta|,$$

$$|^3T_{1\gamma}\rangle = |v\bar{u}u\zeta|$$

$^5E(t_2^3e)$

$$|^5E_u\rangle = -|\xi\eta\zeta v|, \quad |^5E_v\rangle = |\xi\eta\zeta u|$$

Matrix Elements of the Crystal-Field Operator on the Basis of the $^3T_1$ States.

$^3T_1(t_2^4)$

$$\langle^3T_{1\alpha}|V_{cr}|^3T_{1\alpha}\rangle = 388 - 5458G, \quad \langle^3T_{1\beta}|V_{cr}|^3T_{1\beta}\rangle = 388 - 5458G,$$

$$\langle^3T_{1\gamma}|V_{cr}|^3T_{1\gamma}\rangle = -4387 - 5856G$$

$^3T_1[t_2^3(^2T_1)e]$

$$\langle^3T_{1\alpha}|V_{cr}|^3T_{1\alpha}\rangle = -2419 - 2534G, \quad \langle^3T_{1\beta}|V_{cr}|^3T_{1\beta}\rangle = -2419 - 2534G,$$

$$\langle^3T_{1\gamma}|V_{cr}|^3T_{1\gamma}\rangle = 3485 - 1222G$$

$^3T_1[t_2^3(^2T_2)e]$

$$\langle^3T_{1\alpha}|V_{cr}|^3T_{1\alpha}\rangle = 1517 - 1659G, \quad \langle^3T_{1\beta}|V_{cr}|^3T_{1\beta}\rangle = 1517 - 1659G,$$

$$\langle^3T_{1\gamma}|V_{cr}|^3T_{1\gamma}\rangle = -4387 - 2971G$$

$^3T_1[t_2^2(^3T_1)e^2(^1A_1)]$

$$\langle^3T_{1\alpha}|V_{cr}|^3T_{1\alpha}\rangle = -1291 + 1265G,$$

$$\langle^3T_{1\beta}|V_{cr}|^3T_{1\beta}\rangle = -1291 + 1265G,$$

$$\langle^3T_{1\gamma}|V_{cr}|^3T_{1\gamma}\rangle = 3485 + 1663G$$

$^3T_1[t_2^2(^3T_1)e^2(^1E)]$

$$\langle^3T_{1\alpha}|V_{cr}|^3T_{1\alpha}\rangle = -1291 + 1265G,$$

$$\langle^3T_{1\beta}|V_{cr}|^3T_{1\beta}\rangle = -1291 + 1265G,$$

$$\langle^3T_{1\gamma}|V_{cr}|^3T_{1\gamma}\rangle = 3485 + 1663G$$

$^3T_1[t_2^2(^3T_1)e^2(^3A_2)]$

$$\langle^3T_{1\alpha}|V_{cr}|^3T_{1\alpha}\rangle = -1291 + 1265G,$$

$$\langle^3T_{1\beta}|V_{cr}|^3T_{1\beta}\rangle = -1291 + 1265G,$$

$$\langle^3T_{1\gamma}|V_{cr}|^3T_{1\gamma}\rangle = 3485 + 1663G$$

$^3T_1(t_2e^3)$

$$\langle^3T_{1\alpha}|V_{cr}|^3T_{1\alpha}\rangle = 677 + 4587G,$$

$$\langle^3T_{1\beta}|V_{cr}|^3T_{1\beta}\rangle = 677 + 4587G,$$

$$\langle^3T_{1\gamma}|V_{cr}|^3T_{1\gamma}\rangle = 1805 + 5502G$$

$^5E(t_2^3e)$

$$\langle^5E_u|V_{cr}|^5E_u\rangle = -4387 - 2971G,$$

$$\langle^5E_v|V_{cr}|^5E_v\rangle = 3485 - 1222G \qquad \text{(A7)}$$

AUTHOR INFORMATION

Corresponding Author

*E-mail: klokishner@yahoo.com.

ACKNOWLEDGMENT

S.I.K. and O.S.R. gratefully acknowledge financial support of the STCU (Project N 5062) and the Supreme Council on Science and Technological Development of Moldova.

REFERENCES

(1) Cambi, L.; Szego, L.; Cagnasso, A. *Atti Accad. Naz. Lincei, Cl. Sci. Fis., Mat. Nat., Rend.* **1931**, *13*, 168.

(2) Cambi, L.; Szego, L. *Atti Accad. Naz. Lincei, Cl. Sci. Fis., Mat. Nat., Rend.* **1931**, *15*, 329.

(3) Cambi, L.; Szego, L. *Atti Accad. Naz. Lincei, Cl. Sci. Fis., Mat. Nat., Rend.* **1932**, *15*, 599.

(4) Gütlich, P.; Hauser, A.; Spiering, H. *Angew. Chem., Int. Ed. Engl.* **1994**, *33*, 20.

(5) Gütlich, P.; Garcia, Y.; Goodwin, H. A. *Chem. Soc. Rev.* **2000**, *29*, 419.

(6) Hauser, A. *Coord. Chem. Rev.* **1991**, *111*, 275.

(7) Gütlich, P.; Goodwin, H. A. *Spin Crossover in Transition Metal Compounds*; Springer-Verlag: Berlin, 2004.

(8) Hauser, A. *Light-Induced Spin Crossover and the High-Spin → Low-Spin Relaxation*; Springer-Verlag: Berlin, 2004.

(9) Gütlich, P.; Ksenofontov, V.; Gaspar, A. B. *Coord. Chem. Rev.* **2005**, *249*, 1811.

(10) Spiering, H.; Meissner, E.; Köppen, H.; Müller, E. W.; Gütlich, P. *Chem. Phys.* **1982**, *68*, 65.

(11) Wajnflasz, J.; Pick, R. *J. Phys. (Paris), Colloq.* **1971**, *32*, C1–91.

(12) Bousseksou, A.; Nasser, J.; Linares, J.; Boukheddaden, K.; Varret, F. *J. Phys. I (France)* **1992**, *2*, 1381.

(13) Bousseksou, A.; Varret, F.; Nasser, J. *J. Phys. I (France)* **1993**, *3*, 1463.

(14) Bousseksou, A.; Constant-Machado, J.; Varret, F. *J. Phys. I (France)* **1995**, *5*, 747.

(15) Boukheddaden, K.; Shteto, I.; Hôo, B.; Varret, F. *Phys. Rev. B* **2000**, *62*, 14796. *62*, 14806.
(16) Nishino, M.; Miyashita, S.; Boukheddaden, K. *J. Chem. Phys.* **2003**, *118*, 4594.
(17) Nishino, M.; Boukheddaden, K.; Miyashita, S.; Varret, F. *Phys. Rev. B* **2005**, *72*, 064452.
(18) Miyashita, S.; Konishi, Y.; Tokoro, H.; Nishino, M.; Boukheddaden, K.; Varret, F. *Prog. Theor. Phys.* **2005**, *114*, 719.
(19) Sim, P. G.; Sinn, J. *J. Am. Chem. Soc.* **1981**, *103*, 241.
(20) Halepoto, D. M.; Holt, D. G. L.; Larkworthy, L. F.; Leigh, G. L.; Povey, D. C.; Smith, G. W. *J. Chem. Soc., Chem. Commun.* **1989**, 1322.
(21) Murray, K. S. *Eur. J. Inorg. Chem.* **2008**, 3101.
(22) Garcia, Y.; Gütlich, P. *Top. Curr. Chem.* **2004**, *234*, 786.
(23) Zelentsov, V. V.; Somova, I. K. *Zh. Obshch. Khim.* **1974**, *44*, 1309.
(24) Morgan, G. G.; Murnaghan, K. D.; Müller-Bunz, H.; McKee, V.; Harding, C. J. *Angew. Chem., Int. Ed.* **2006**, *45*, 7192.
(25) Garcia, Y.; Kahn, O.; Ader, J.-P.; Buzdin, A.; Meurdesoif, Y.; Guillot, M. *Phys. Lett. A* **2000**, *271*, 145.
(26) Nakano, M.; Matsubayshi, G.; Matsuo, T. *Phys. Rev. B* **2002**, *66*, 212412.
(27) Kimura, S.; Narumi, Y.; Kindo, D.; Nakano, M.; Matsubayshi, G. *Phys. Rev. B* **2005**, *72*, 064448.
(28) Nakano, M.; Matsubayashi, G.; Matsuo, T. *Adv. Quantum Chem.* **2003**, *44*, 617.
(29) Liu, Z.; Liang, S.; Di, X.; Zhang, J. *Inorg. Chem. Commun.* **2008**, *11*, 783.
(30) Wang, S.; Ferbinteanu, M.; Marinescu, C.; Dobrinescu, A.; Ling, Q.-D.; Huang, W. *Inorg. Chem.* **2010**, *49*, 9839.
(31) Garcia, Y.; Paulsen, H.; Schünemann, V.; Trautwein, A. X.; Wolny, J. A. *Phys. Chem. Chem. Phys.* **2007**, *9*, 1194.
(32) Stratt, R. M.; Adachi, S. H. *J. Chem. Phys.* **1987**, *86*, 7156.
(33) Bersuker, I. B. *The Jahn−Teller Effect and Vibronic Interactions in Modern Chemistry*; Plenum: New York, 1984.
(34) Popova, M. N.; Chukalina, E. P.; Malkin, B. Z.; Saikin, S. K. *Phys. Rev. B* **2000**, *61*, 7421.
(35) Klokishner, S.; Melsheimer, J.; Jentoft, F. C.; Schlögl, R. *Phys. Chem. Chem. Phys.* **2004**, *6*, 2066.
(36) Klokishner, S. I.; Tsukerblat, B. S.; Reu, O. S.; Palii, A. V.; Ostrovsky, S. M. *Chem. Phys.* **2005**, *316*, 83.
(37) Klokishner, S. I.; Tsukerblat, B. S.; Reu, O. S.; Palii, A. V.; Ostrovsky, S. M. *Opt. Mater.* **2005**, *27*, 1445.
(38) Klokishner, S. I.; Reu, O. S.; Ostrovsky, S. M.; Palii, A. V.; Kulyuk, L. L.; Tsukerblat, B. S.; Towe, E. *J. Mol. Struct.* **2007**, *838*, 133.
(39) Klokishner, S.; Reu, O.; Ostrovsky, S.; Palii, A.; Towe, E. *J. Phys.: Condens. Matter* **2007**, *19*, 486213.
(40) Abragam, A.; Bleaney, B. *Electron paramagnetic resonance of transition ions*; Clarendon Press: Oxford, U.K., 1970.
(41) Clementi, E.; Roetti, C. *At. Data Nucl. Data Tables* **1974**, *14*, 177.
(42) Sugano, S.; Tanabe, Y.; Kamimura, H. *Multiplets of transition-metal ions in crystals*; Academic Press: New York, 1970.
(43) Biernach, S. W.; Kaminska, A.; Suchocki, A.; Arizmendi, L. *Appl. Phys. Lett.* **2002**, *81*, 442.
(44) Bersuker, I. B.; Vekhter, B. G. *Fizica Tverdogo Tela* **1963**, *5*, 2432.
(45) Ham, F. S. *Phys. Rev. A* **1965**, *138*, 1727.
(46) Ham, F. S. *Phys. Rev.* **1965**, *166*, 307.
(47) Klokishner, S. I.; Varret, F.; Linares, J. *Chem. Phys.* **2000**, *255*, 317.
(48) Klokishner, S. I.; Linares, J. *Phys. Chem. C* **2007**, *111*, 10644.
(49) Klokishner, S. I. *Chem. Phys.* **2001**, *269*, 411.
(50) Kanamori, J. *J. Appl. Phys.* **1960**, *31*, 145.
(51) Gehring, G. A.; Gehring, K. A. *Rep. Prog. Phys.* **1975**, *38*, 1.
(52) Slichter, C. P.; Drickamer, H. G. *J. Chem. Phys.* **1972**, *56*, 2142.
(53) Sorai, M.; Seki, S. *J. Phys. Chem. Solids* **1974**, *35*, 5550.
(54) Bousseksou, A.; McGarvey, J.; Varret, F.; Real, J. A.; Tuchagues, J. P.; Dennis, A. C.; Boillot, M. L. *Chem. Phys. Lett.* **2000**, *318*, 409.
(55) Enachescu, C.; Linares, J.; Varret, F. *J. Phys.: Condens. Matter* **2001**, *13*, 2481.